Metals and Materials International (2022) 28:618–627
https://doi.org/10.1007/s12540-020-00911-6

Effect of Cooling Rates from Solution Treatment Temperature on Aging Response and Fracture Behavior of a Mg–8Al–0.5Zn Alloy

A. Zindal[1] · H. Vashishtha[1] · S. S. Singh[2] · R. Prasad[1] · J. Jain[1]

Received: 9 September 2020 / Accepted: 22 October 2020 / Published online: 3 January 2021

Abstract
In the present study, a Mg–8Al–0.5Zn (AZ80) Mg alloy was subjected to water quenching and furnace cooling from the solution treatment temperature of 390 °C. Subsequently, all the samples were subjected to aging treatment at 250 °C. The precipitation behavior, aging response and fracture phenomenon of the AZ80 Mg alloy were evaluated to establish the correlation among the cooling rates after solution treatment, microstructural features and mechanical properties. Scanning electron microscopy depicted a very distinct precipitation behavior of aged specimens. The observed variation in the aging curves was rationalized based on this. Fractographic analysis on the as-solutionized and aged alloys revealed that the initiation of fracture (i.e., intergranular or transgranular) was dictated by the presence of microstructural features, such as precipitates (continuous and discontinuous), twins and grain boundaries. The fracture strain was correlated with the number density and size of voids formed during tensile loading.

Keywords AZ80 Mg alloy · Cooling routes · Aging response · Continuous and discontinuous precipitates · Fracture phenomenon

1 Introduction

Among various commercial alloys, the AZ series (Mg–Al based alloy system) is widely employed in industrial applications, such as automotive wheels, extruded sections etc. [1]. Aging treatment is considered as a vital process to optimize the microstructural features and subsequently tailor the mechanical properties. The microstructure of the Mg–Al alloy possesses α-Mg phase and intermetallic β-$Mg_{17}Al_{12}$ precipitates in the as-cast condition [2, 3]. The precipitation of β-phase occurs in two forms viz. continuous and discontinuous precipitates. The continuous precipitates (CP) are nucleated and grown at the grain boundaries and within the grains in a plate shaped morphology, whereas the discontinuous precipitates (DP) are developed at high angle boundaries of the α-Mg phase and grown in a cellular manner with lamellar morphology towards the other grain [2, 4–6]. Furthermore, the ellipsoidal morphology of discontinuous precipitates has also been reported for the Mg–Al alloy [7]. The continuous precipitates are considered to be more effective in strengthening as compared to the discontinuous precipitates owing to the coarser nature of latter than the former [4, 5, 8–10]. Moreover, the large-sized brittle $Mg_{17}Al_{12}$ precipitates are reported to be the regions of stress concentration, which facilitate the nucleation of voids at the interface of the β-$Mg_{17}Al_{12}$ and α-Mg matrix or particle fracture during plastic deformation [11–13]. With the coalescences of voids, cracks are formed both at the grain boundaries and within the grains [14].

A significant amount of work has been carried out on the variation of precipitate characteristics with a cooling medium after the solution treatment in the Al alloys [15–18]. For example, Unwin and Nicholson [15] and Embury and Nicholson [16] observed that the slower cooling rates (oil quenching) after the solution treatment resulted in the formation of few coarser precipitates as compared to water quenching in the Al–Zn–Mg alloys. Rosenbaum and Turnbull [17] reported the formation of a higher number density of particles for the faster cooling rate (water quenching) as compared to the slower rate (air cooling) for the Al–Si alloy

✉ J. Jain
jayantj@iitd.ac.in

[1] Department of Materials Science and Engineering, Indian Institute of Technology, Delhi, New Delhi 110016, India

[2] Department of Material Science and Engineering, Indian Institute of Technology Kanpur, Kanpur, Uttar Pradesh 208016, India

system. However, very few studies have been performed to understand the effect of varying cooling rates on the precipitation behavior for the Mg–Al alloys. For instance, Braszczyńska-Malik [3] observed the formation of discontinuous precipitates at a slower cooling rate (5 K/min) after the solution treatment for the AZ91 alloy. In contrast, Zhang and Kelly [19] noticed the formation of pearlite shaped of continuous precipitates after the furnace cooling.

Furthermore, in the Mg–Al alloy system, precipitate characteristics are reported to regulate the tensile response. For instance, Patel et al. [20] compared the tensile behavior of thixomolded AZ91D and AM60B Mg alloys and ascribed the improvement in the ductility and reduction in the value of the yield strength to the lower amount of β-$Mg_{17}Al_{12}$ phase for the AM60B alloy. Yakubtsov et al. [21] also reported a similar trend of strength and ductility by comparing the AZ80 Mg alloys in as-cast and solutionized states and rationalized it to the dissolution of the $Mg_{17}Al_{12}$ precipitates. Niknejad et al. [11] related the increase in the weld strength to the elimination of grain boundary β-$Mg_{17}Al_{12}$ precipitates in the resistance spot-welded AZ80 Mg alloy. Zindal et al. [22] attributed the variation in the fracture behavior of the aged AZ80 alloys to the characteristics of the grain boundary precipitates (area fraction and size) and the number density of precipitates formed within the grain.

It is clear that the effect of precipitate characteristics (type, size, morphology, number density and distribution) on the aging response and subsequently on the fracture phenomenon at varying cooling routes, after the solution treatment, for the Mg–Al alloy system are still scanty. Therefore, in the present study, the precipitation behavior of the AZ80 alloy has been evaluated at two different cooling routes: water quenching (W/Q) and furnace cooling (F/C) after solution treatment temperature. In addition, the relationship between the precipitate characteristics and the fracture behavior (i.e., types of cracks, strain to fracture and voids features) has been studied.

2 Experimental Procedure

The as-cast AZ80 (Mg–8 wt%Al–0.5 wt%Zn) Mg alloy was used as a starting material. The alloy was first solutionized at 390 °C for 24 h and cooled in two different ways (water quenching and furnace cooling) with an approximate cooling rate of ~ 10,000 K/s and ~ 0.3 K/s, respectively [23]. Further, the aging was performed at 250 °C for varying time duration. The microstructures of the as-cast, solutionized and aged samples were characterized with an optical microscope (Carl Zeiss) and scanning electron microscope (FEI Quanta 200 F FESEM). Samples were first prepared with standard metallographic techniques, followed by chemical etching in 10% Nital solution and subsequently with 10% HF solution for ~ 5 s. Micro-hardness was measured using a Vickers micro-hardness tester (HMV2, Shimadzu) with a 3 N load for a dwell time of 10 s. The reported value of hardness was the average of the eight equally spaced indentations made on the polished sample surface. To examine the fracture behavior, a 30 KN capacity screw driven Zwick tensile machine was used to perform the uniaxial tensile test at a constant strain rate of 0.001 s^{-1} at room temperature. The testing was carried out on the pre-polished and etched samples. Tensile samples were prepared by electric discharge machining (EDM) according to ASTM: E8/E8M standard [24]. The elongation was measured with a video extensometer (non-contact mode) attached to the machine. After testing, fractography was performed using a SEM (TM3000, Hitachi). Quantitative assessment of voids density was carried out using Image J software, where at least eight different fractographs were considered for each condition. It is noteworthy here that in determining the fracture response of aged condition, an over-aged state at 250 °C has been considered.

3 Results and Discussion

3.1 As-Cast and Solution Treated Microstructures

The micrograph of the as-cast AZ80 alloy composed of α-Mg matrix and β-$Mg_{17}Al_{12}$ precipitates developed predominantly along the grain boundaries, as depicted in Fig. 1a. The dissolution of the β-$Mg_{17}Al_{12}$ precipitates in the matrix and the formation of an equiaxed grain structure is observed for as-solutionized specimen quenched in water (Fig. 1b). In contrast, the furnace cooled specimen depicts the discontinuous precipitates of β-$Mg_{17}Al_{12}$ in lamellar morphology, as shown in Fig. 1c. The formation of discontinuous precipitates for furnace cooled alloy can be ascribed to the preferential accumulation of solutes at the grain boundaries. This may be related to the fact that the grain boundaries provide the heterogeneous nucleation sites for the precipitation. At the slower cooling rate, the solutes present in the vicinity of grain boundaries are likely to be diffused there and form precipitates through the mechanism of grain boundary diffusion [15]. With continuing precipitation, the precipitates grow in size and further, branching of the precipitates takes place leading to the cellular structure [25]. On the contrary, faster cooling rates associated with the water quenched specimen do not possess enough time for the solutes to accumulate at the grain boundaries and form precipitates.

3.2 Effect of Cooling Rate on the Aging Response and Precipitation Behavior

Figure 2 depicts the aging curves at 250 °C for both the cooling rates. It can be observed that the peak hardness for the

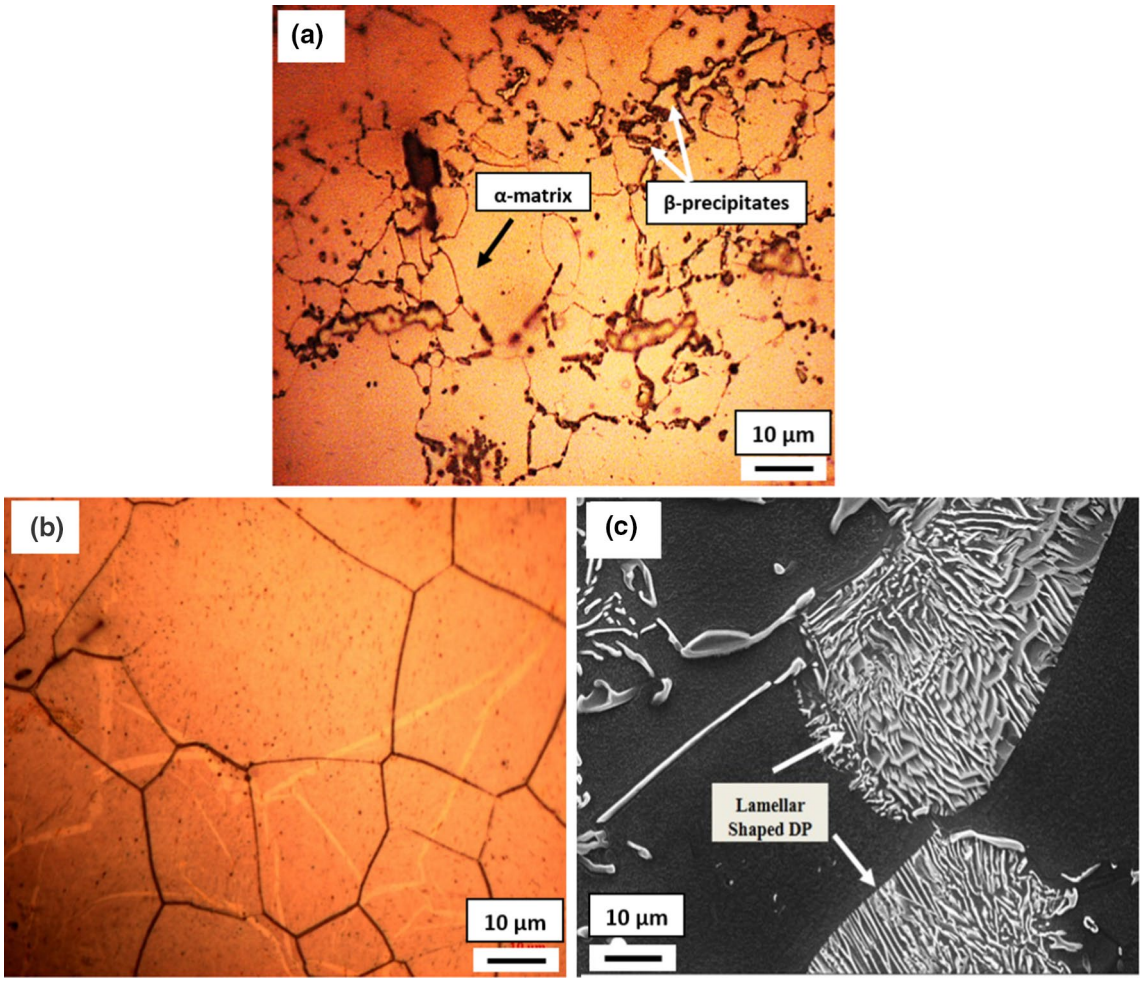

Fig. 1 Optical micrographs of **a** as-cast alloy, **b** as-solutionized alloy quenched in water, and **c** SEM micrograph of a furnace cooled solutionized alloy. Note that **c** illustrates the formation of the discontinuous precipitates (DP)

water quenched and furnace cooled alloys were achieved at 16 h and 24 h, respectively. The lower peak hardness time in the water quenched alloy can be attributed to the faster nucleation rate of precipitates owing to the presence of non-equilibrium concentration (as-quenched) of vacancies and solute supersaturation. In addition, the hardness values for the water quenched alloys, at all the aging times, are higher than the furnace cooled alloys. For instance, the peak and over-aged (48 h) hardness values for the water quenched alloy are ~ 79.7 and ~ 75.5 HV, respectively, whereas for the furnace cooled alloy they are reduced to ~ 76.2 HV and ~ 69.8 HV, respectively. This will be discussed in more detail in the following sections. Nevertheless, it should be noted that the increase in the value of peak hardness with an increase in the cooling rate has also been observed by Gill et al. [26] for the Mg–Nd–Gd–Zr alloy system.

Figure 3 illustrates the precipitation behavior of the furnace cooled and water quenched alloys at under-aged, peak-aged and over-aged conditions. For the furnace cooled

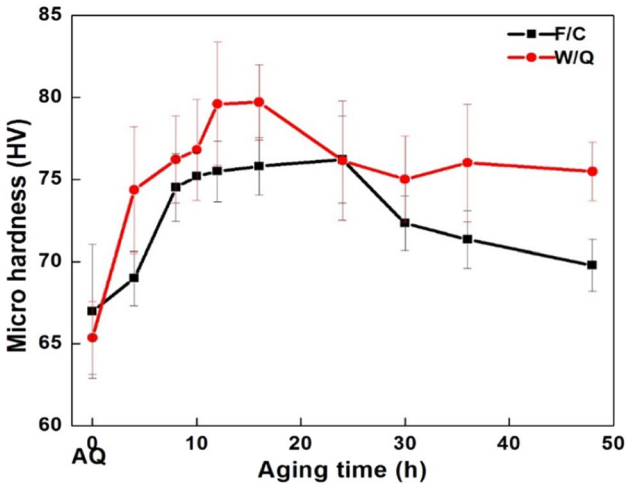

Fig. 2 The aging response of water quenched (W/Q) and furnace cooled (F/C) alloys aged at 250 °C. The "AQ" indicates the as-quenched condition

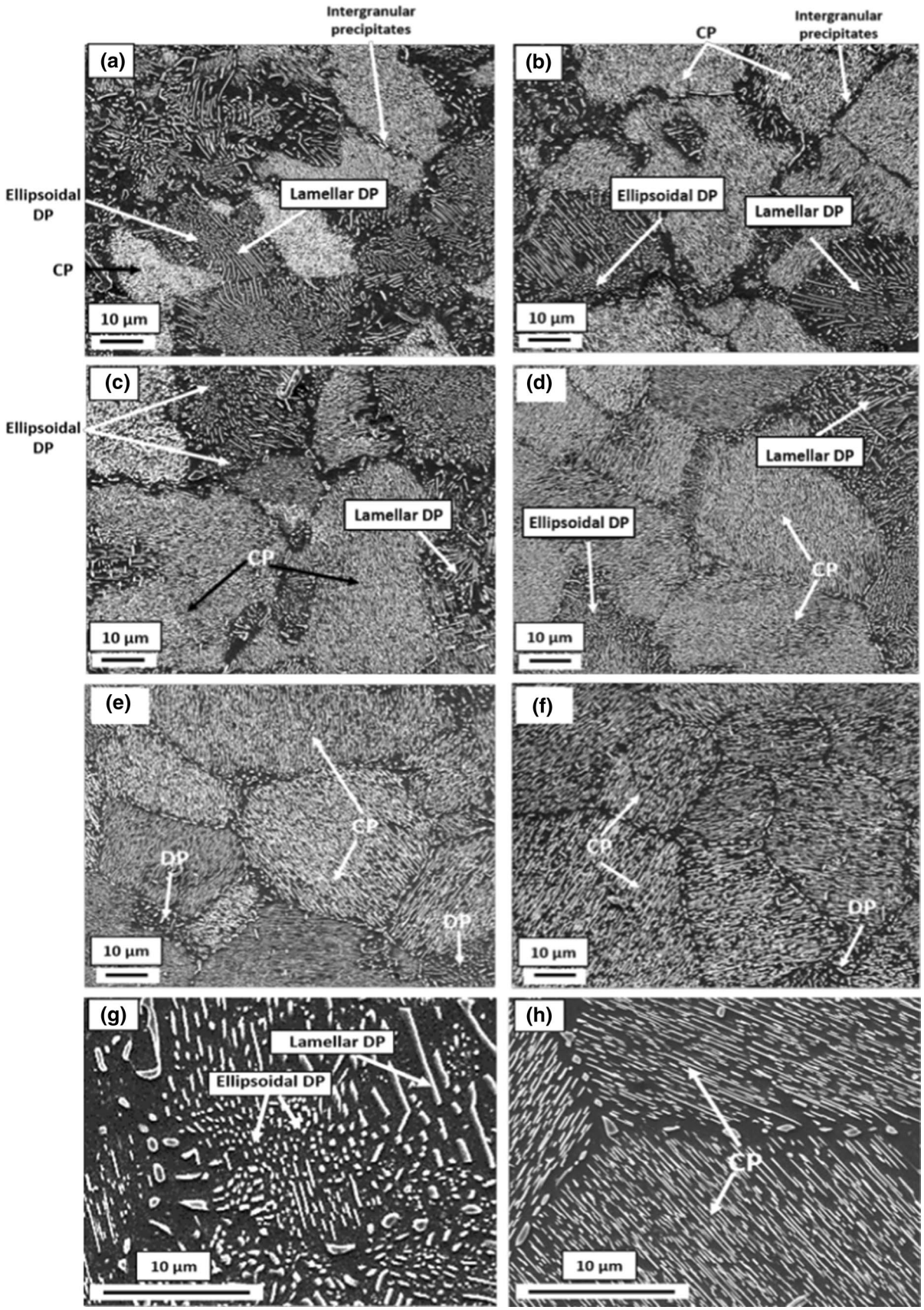
(a)
Intergranular precipitates
Ellipsoidal DP
Lamellar DP
CP
10 µm
(b)
CP
Intergranular precipitates
Ellipsoidal DP
Lamellar DP
10 µm
(c)
Ellipsoidal DP
Lamellar DP
CP
10 µm
(d)
Lamellar DP
Ellipsoidal DP
CP
10 µm
(e)
CP
DP
DP
10 µm
(f)
CP
DP
10 µm
(g)
Lamellar DP
Ellipsoidal DP
10 µm
(h)
CP
10 µm

◂**Fig. 3** SEM images illustrating the precipitates characteristics in the furnace cooled alloys, aged at 250 °C for **a** under-aged (12 h), **b** peak-aged (24 h), and **c** over-aged (48 h). The images of the water quenched alloys: **d** under-aged (4 h), **e** peak-aged (16 h), and **f** over-aged (48 h). **g**, **h** are the higher magnification SEM images of peak-aged condition of furnace cooled and water quenched alloys, respectively. In **g**, the ellipsoid shaped discontinuous precipitates can also be observed. Note that, the 'CP' and 'DP' stand for the continuous and discontinuous precipitates, respectively

alloy, it can be observed that both types of precipitates, i.e., continuous (both at the grain boundary and within the grain) as well as discontinuous are formed at all the aging times, as shown in Fig. 3a–c. Additionally, the discontinuous precipitates are observed to form in lamellar and ellipsoidal morphologies. The aforementioned morphologies of the precipitates are also observed to form in the water quenched alloys (Fig. 3d–f). However, the number density of the continuous precipitates appears to be more and the distribution of precipitates seems to be finer as compared to the furnace cooled alloys (Fig. 3d–f). In order to illustrate this more explicitly, the higher magnification images of the peak-aged condition for furnace cooled and water quenched alloys are compared in Fig. 3g, h, respectively.

Qualitatively, it can also be noted that for both the differently cooled alloys, with an increase in the aging time, the number density of the continuous precipitates was also observed to increase (Fig. 3). For the over-aged alloys, the continuous precipitates seemed to occupy all the regions except those where the discontinuous precipitates were observed (Fig. 3c, f). This can be attributed to the formation of the continuous precipitates which reduced the driving energy for the growth of the discontinuous precipitates [3, 13, 27].

The difference in the precipitation behavior with the varying cooling rates, shown in Fig. 3, can be attributed to the presence of more lattice defects, such as vacancies, in the matrix and the decomposition of a supersaturated solid solution of the water quenched alloys. Many authors have reported the presence of the non-equilibrium vacancy concentration after the solutionizing and quenching treatment for the Al alloys [16–18]. Considering a method proposed by Embury and Nicholson [16], Zindal et al. [28] determined the vacancy concentration profile in the AZ80 Mg alloy for various cooling mediums. In this approach, the vacancy concentration was calculated with varying distance from the grain boundary at a particular solutionizing temperature and quenching rate, keeping the other parameters constant. Figure 4 depicts the vacancy concentration profiles, determined in the same manner, at two different cooling rates (i.e., 10,000 K/s and 0.3 K/s) by taking the solutionizing temperature as 390 °C. It can be observed that for the faster cooling rate (water), the vacancy concentration profile is significantly higher than that observed at the slower rate (furnace cooling) for all the distances (Fig. 4). A similar trend of the vacancy concentration profiles with varying cooling rates was also observed for the Al–Zn–Mg alloy [16]. For the Mg–Al [3] and Al–Zn–Mg [16] alloys, the increased vacancy concentration was found to enhance the nucleation rate of precipitates through the volume diffusion mechanism at a given temperature. It is noteworthy that the quenched-in vacancies are diminished with time during aging [25]. Moreover, in the water quenched sample, owing to the faster rate of cooling (as negligible solute will come out due to faster cooling) the supersaturated solid solution is developed. This leads to the higher driving force for the nucleation of precipitates, results in the enhanced number density of continuous precipitates during the aging treatment. Whereas, during the furnace cooling, owing to the formation of discontinuous precipitates, the solute supersaturation is decreased. This causes the formation of a lower number density of continuous precipitates. In this study, a higher number density of the continuous precipitates in the water quenched alloys (Fig. 3d–f) as compared to the furnace cooled alloy can also be ascribed to the higher vacancy concentration and solute supersaturation in the former.

The above-mentioned differences in the precipitate characteristics of the aged alloys can be used to understand the observed differences in their aging responses (Fig. 2). It has been observed that higher number density and finer distribution of continuous precipitates result in the higher hardness of the alloy [9]. Further, Lai et al. [7] stated that the coarser distribution of ellipsoidal shaped precipitates leads to the reduction in the hardness of the Mg–Al alloys. In the present work, the higher number density and finer distribution of the continuous precipitates in the water quenched alloys (Fig. 3d–f) and coarser distribution with the higher number density of the discontinuous precipitates in the furnace cooled alloys (Fig. 3a–c) resulted in the observed trend in the hardness values (Fig. 2).

3.3 Fracture Characteristics

3.3.1 Fracture Response of the As-Solutionized Alloys

Figure 5a shows the true stress-strain curves of the as-solutionized alloys for both cooling routes. For the as-solutionized state (Fig. 5a), the total strain to fracture increases substantially (~28%) from the furnace cooled (having value 6.8%) to water quenched alloy (with value 8.7%). This can be rationalized in terms of the voids characteristics, which will be explained later (Sect. 3.3.3). Furthermore, the value of the fracture stress is measured to be higher ~14% for the water quenched alloy (value ~255 MPa) than the furnace cooled alloy (value ~223 MPa).

The fracture characteristics of the as-solutionized alloys after furnace cooling and water quenching, examined on the

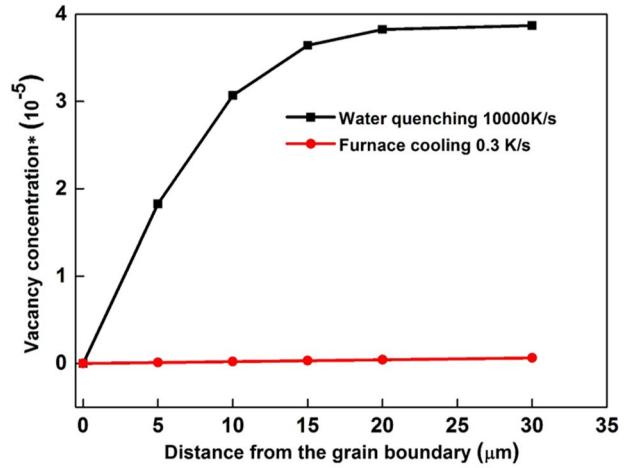

Fig. 4 Vacancy concentration profiles for the furnace cooled and water quenched alloys from solutionizing temperature of 390 °C

pre-polished etched surface parallel to the tensile axis, are shown in Fig. 6a, b, c, d, respectively. It can be observed that both types of cracks, i.e., intergranular (IG) and transgranular (TG) are formed on both the alloys. In addition, the presence of the voids at the precipitate/matrix interface could also be noticed in the furnace cooled alloy (Fig. 6a, b). The appearance of the cracks (IG and TG) on the fracture surface of the furnace cooled alloy can be attributed to the coalescence of voids, nucleated either at the interface of the precipitate-matrix (at the grain boundary and within the grain) or at the site of the precipitate cracking [11, 22]. Contrary to this, basal slip and $\{10\bar{1}2\}$ twins are considered to be responsible for the nucleation of cracks in the water quenched alloys (Fig. 6c, d). In the absence of the precipitates, the movement of dislocations could be restricted at

Fig. 6 SEM micrographs of the as-solutionized alloys showing the fracture characteristics after **a**, **b** furnace cooling, and **c** water quenching. **d** illustrates the presence of slip and twins clearly in the water quenched alloy. The 'IG' and 'TG' correspond to the intergranular and transgranular, respectively. **e**, **f** are the SEM fractographs of the furnace cooled and water quenched alloys, respectively. **g** shows the number density of voids for the furnace cooled and water quenched as-solutionized conditions

the grain boundaries and twins, resulting in the piling up of dislocations [29]. This may cause the onset of stress concentration, and therefore formation of cracks, at the grain boundaries and twin/matrix interfaces. As a consequence, the intergranular and transgranular cracks might initiate and grow along the grain boundaries and twins, respectively. The growth of the transgranular cracks along the twin/matrix interface has also been reported for the AZ91 Mg alloy [30].

The representative SEM fractographs of the as-solutionized alloys, with the presence of varying size of voids, are shown in Fig. 6e, f. A remarkable increase in the number density of voids (~59%) is detected for the furnace cooled alloy (Fig. 6g). As mentioned, this could be ascribed to the presence of precipitates (Fig. 1c).

The observed higher stress and fracture strain of the water quenched alloy, as compared to the furnace cooled alloy (Fig. 5a) can be ascribed to the presence of twins and solutes. Niknejad et al. [11] mentioned that the growth of cracks was retarded owing to the formation of extensive twinning before the fracture of the as-solutionized AZ80 alloy having no precipitates. Furthermore, for the as-solutionized state, the dissolution of precipitates after the solution treatment enhanced the hardening effect owing to the formation of a supersaturated solid solution [11]. Therefore, it might be reasonable to deduce that the combined effect of solid-solution hardening and strengthening due to twins

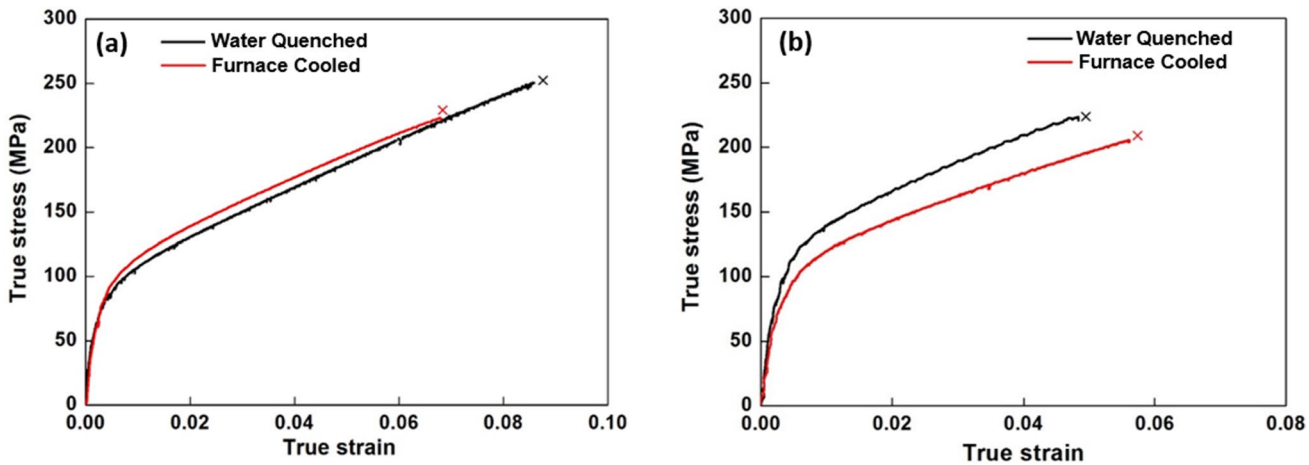

Fig. 5 True stress–strain curves of the furnace cooled and water quenched alloys for the **a** as-solutionized condition and **b** aged condition (250 °C, 48 h). The "cross-marks" denote the points of failure

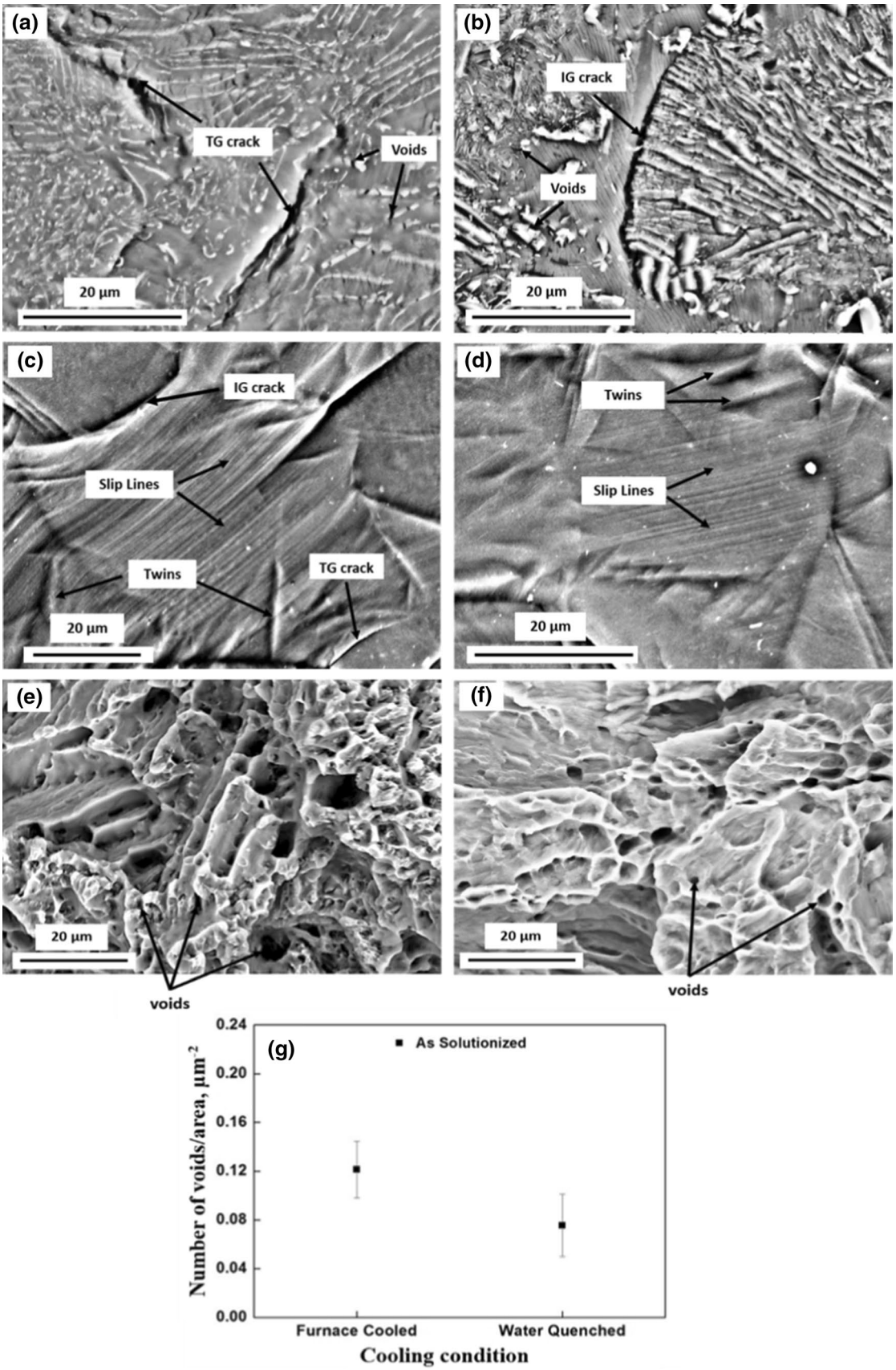
(a)
TG crack
Voids
20 µm
(b)
IG crack
Voids
20 µm
(c)
IG crack
Slip Lines
Twins
TG crack
20 µm
(d)
Twins
Slip Lines
20 µm
(e)
20 µm
voids
(f)
20 µm
voids
(g)
As Solutionized
Number of voids/area, µm-2
0.24
0.20
0.16
0.12
0.08
0.04
0.00
Furnace Cooled
Water Quenched
Cooling condition

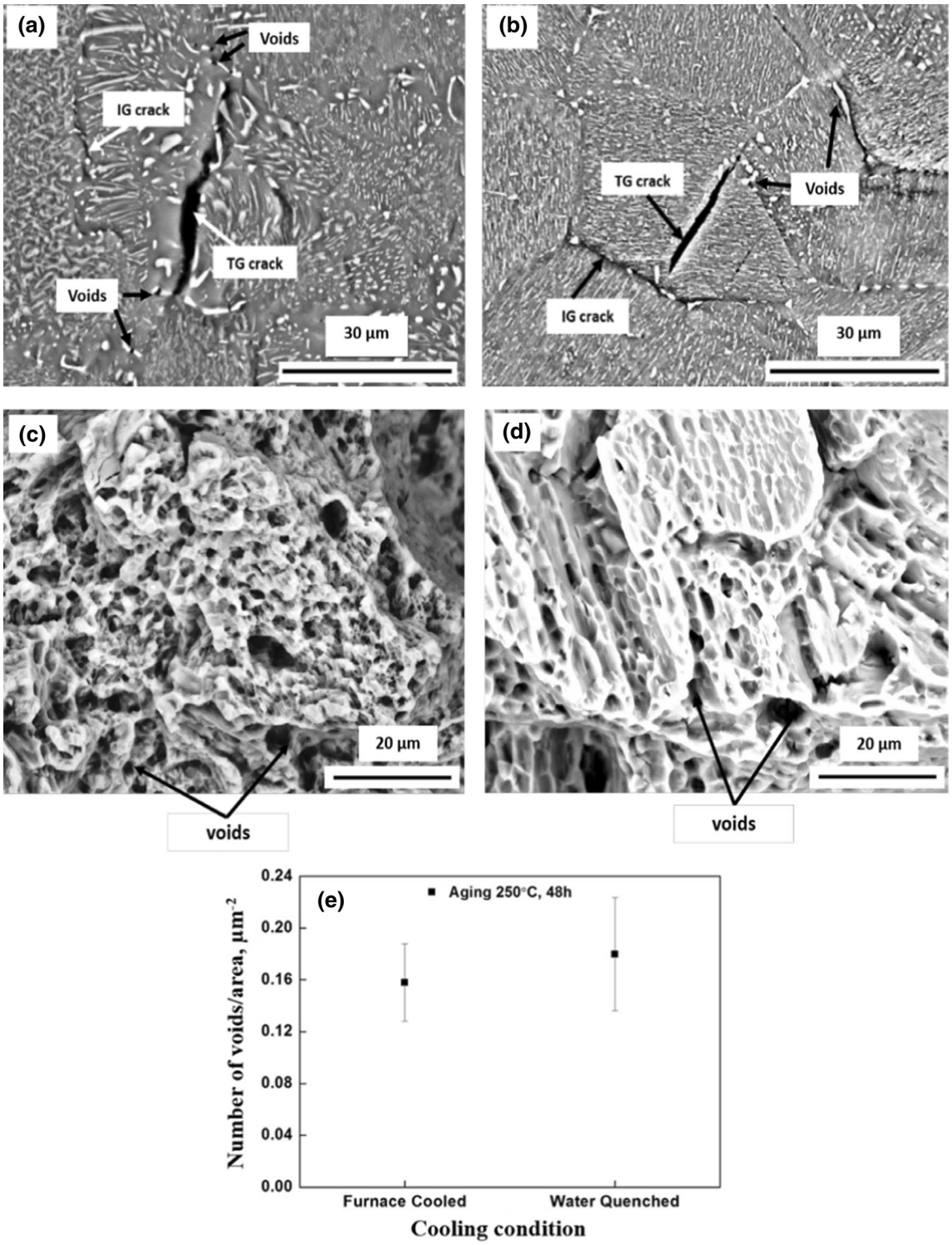

Fig. 7 SEM images of the aged alloys (250 °C, 48 h) exhibiting the fracture behavior after **a** furnace cooling and **b** water quenching. **c**, **d** are the fractographs after furnace cooling and water quenching, respectively. **e** shows the comparison of the voids density between the aged alloys after furnace cooling and water quenching

could be rationalized for the observed increased value of fracture stress and subsequently fracture strain for the water quenched as-solutionized state (Fig. 5a).

3.3.2 Fracture Response of Aged Alloys

The true stress-strain curves of the water quenched and furnace cooled alloys, aged at 250 °C for 48 h, are illustrated in Fig. 5b. The fracture strain (~5.6%) of the furnace cooled alloy is ~16% higher than the fracture strain of the water quenched alloy (~4.8%), whereas the fracture stress is marginally higher (~7%) for the water quenched alloy. The rationale behind the difference in the fracture strain values of both the aged alloys will be discussed later (Sect. 3.3.3). The fracture characteristics of both the aged alloys (Fig. 7a, b), analyzed on the surface parallel to the tensile axis, manifest the occurrence of IG as well as TG cracks. The number density of voids (Fig. 7e), determined using the fractographs (Fig. 7c, d), is marginally higher (~14%) in the water quenched alloy. For the Mg–Al alloy system, continuous precipitates have been reported to be more effective in determining the strength, the value of which was found to decrease with an increase in the inter-precipitates distance [9, 10]. Therefore, the observed higher value of the fracture stress and number density of voids in the water quenched alloy might be attributed to the higher number density and finer distribution of the continuous precipitates in its microstructure (Fig. 3d–f) as compared to the furnace cooled alloy, where a high density of discontinuous precipitates with coarser distribution is observed (Fig. 3a–c).

3.3.3 Correlation Between Fracture Strain and Void Features

The measured values of the fracture strain and the number density of voids for the different heating conditions are summarized in Fig. 8. It is evident that the fracture strain follows a linear relationship with the number density of voids. It should also be noted that a considerable difference is observed between the fracture response of the as-solutionized and aged alloys. For instance, in the case of the furnace cooled alloys, the observed value of the fracture strain for the as-solutionized sample is ~6.8% (Fig. 8), which increases by ~21% for the aged alloys (~5.6%). Moreover, the number density of voids is ~32% higher for the aged alloy (value ~0.16 μm^{-2}) as compared to the solutionized alloy (value ~0.12 μm^{-2}). In addition, for the as-solutionized sample, qualitatively the voids are observed to be bigger in size (Fig. 6e) than to the aged specimen (Fig. 7c).

The number density and size of the voids have been found to regulate the values of the fracture strain of the Al–Zn–Mg alloy [31]. As mentioned earlier, a higher number density of the continuous precipitates with finer distribution gives

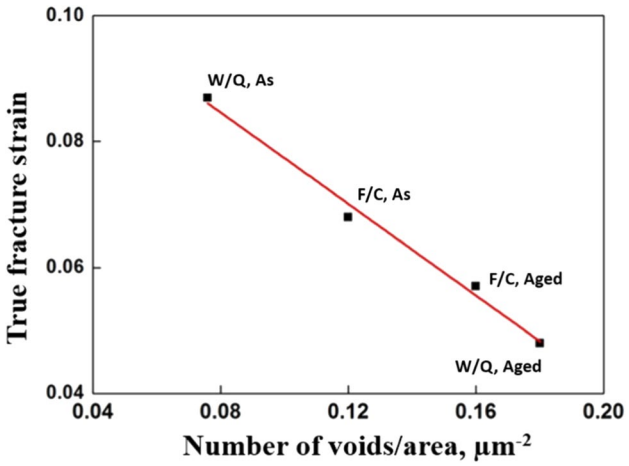

Fig. 8 The relationship between the true fracture strain and the number density of voids for the different heating conditions. The "W/Q, As" refers to water quenched as-solutionized, "F/C, As" refers to furnace cooled as-solutionized, "F/C, Aged" refers to furnace cooled aged (250 °C, 48 h) and "W/Q, Aged" refers to water quenched aged (250 °C, 48 h) alloys

rise to the possibility of the enhancement in the number of inter-phase voids. Therefore, during plastic deformation, the growth of voids is likely to be less owing to their early coalescence with one another. This in turn, leads to the smaller size of voids and rapid commencement of cracks and consequently decreases in the fracture strain. The lower value of fracture strain with the presence of finer voids has also been observed in the Mg alloys [14]. This is consistent with the results shown in Figs. 5b and 7e where, fracture strain is decreased with an increase in the number density of voids for the water quenched alloy, attributed to a higher number of continuous precipitates (Fig. 3d–f). On the contrary, with a lower number density of voids, the voids grow substantially during deformation, resulting in the larger size of voids before their coalescence. Therefore, the cracks are expected to develop at the later stage, leading to a higher value of fracture strain [14, 31]. This behavior is evident in the furnace cooled as-solutionized condition, where the presence of only discontinuous precipitates (Fig. 1c) results in the decreased number density of voids (value ~0.12) with larger size (Fig. 6e) as compared to furnace cooled aged alloy in which the existence of both kinds of precipitates (Fig. 3a–c) leads into the higher number of voids (value ~0.16) with a smaller size (Fig. 7c). A similar explanation related to the fracture strain and voids could also be made to define the observed fracture response of differently cooled as-solutionized conditions (Figs. 5a and 6g). However, for the case of as-solutionized water quenched alloy, the increased fracture strain could also be attributed to the presence of excessive twins before fracture, as mentioned earlier.

4 Conclusions

In this work, the precipitation behavior, aging response and fracture phenomenon of the AZ80 Mg alloy were studied with the varying cooling rates from the solutionizing temperature. The following conclusion can be drawn from the study:

1. The development of discontinuous precipitates is favored at a slower cooling rate, whereas a faster cooling rate promotes the nucleation of continuous precipitates. This is attributed to the difference in the vacancy concentration and solute supersaturation due to the solution treatment.
2. The improvement in the aging response in terms of hardness and kinetics for the water quenched alloy is attributed to the increased rate of the formation of continuous precipitates as compared to the furnace cooled alloy. In addition to the lower number density of continuous precipitates, the coarser distribution of ellipsoidal shaped discontinuous precipitates are the responsible factors for the observed lower hardness of furnace cooled alloys.
3. The fracture response of the aged alloy at varying cooling rates reveals that the presence of β-$Mg_{17}Al_{12}$ precipitates induces the development of both intergranular and transgranular cracks. In contrast, the grain boundaries and twins promote the initiation of both types of cracks in the as-solutionized alloy in the water quenched condition.
4. The higher values of fracture stress and strain to fracture for the as-solutionized water quenched alloys can be rationalised by considering the combined effect of the number density of voids and development of excessive twins before fracture.
5. A decreasing linear relationship is observed between the strain to fracture and the number density of voids. From that, it can be stated that larger voids manifest the increased value of fracture strain.

References

1. M.K. Kulekci, Int. J. Adv. Manuf. Tech. **39**, 851–865 (2008)
2. J.F. Nie, Metall. Mater. Trans. A **43**, 3891–3939 (2012)
3. K.N. Braszczyńska-Malik, J. Alloy. Compd. **477**, 870–876 (2009)
4. L. Jiang, W. Huang, F. Guo, Y. Zhang, D. Zhang, Q. Liu, Mater. Sci. Eng. A **752**, 145–151 (2019)
5. G. Shi, J. Yuan, T. Li, K. Zhang, X. Li, Y. Li, M. Ma, Mater. Sci. Eng. A **774**, 138906 (2020)
6. D. Zhao, Z. Wang, M. Zuo, H. Geng, Mater. Design **56**, 589–593 (2014)
7. W.-J. Lai, Y.-Y. Li, Y.-F. Hsu, S. Trong, W.-H. Wang, J. Alloy. Compd. **476**, 118–124 (2009)
8. C. Wang, R. Xin, D. Li, B. Song, M. Wu, Q. Liu, Mater. Sci. Eng. A **680**, 152–156 (2017)
9. S. Celotto, Acta Mater. **48**, 1775–1787 (2000)
10. P. Yang, L. Wang, Q. Xie, J. Li, H. Ding, L. Lu, Int. J. Min. Met. Mater. **18**, 338–343 (2011)
11. S.T. Niknejad, L. Liu, T. Nguyen, M.-Y. Lee, S. Esmaeili, N.Y. Zhou, Metall. Mater. Trans. A **44**, 3747–3756 (2013)
12. R. Sarvesha, W. Alam, A. Gokhale, T.S. Guruprasad, S. Bhagavath, S. Karagadde, J. Jain, S.S. Singh, Mater. Sci. Eng. A **759**, 368–379 (2019)
13. X. Zhao, S. Li, F. Yan, Z. Zhang, Y. Wu, Materials **12**, 4223 (2019)
14. T.S. Srivatsan, S. Vasudevan, M. Petraroli, J. Alloy. Compd. **461**, 154–159 (2008)
15. P.N.T. Unwin, R.B. Nicholson, Acta Metall. **17**, 1379–1393 (1969)
16. J.D. Embury, R.B. Nicholson, Acta Metall. **13**, 403–417 (1965)
17. H.S. Rosenbaum, D. Turnbull, Acta Metall. **7**, 664–674 (1959)
18. P.N.T. Unwin, G. Lorimer, R.B. Nicholson, Acta Metall. **17**, 1363–1377 (1969)
19. M.X. Zhang, P.M. Kelly, Scripta Mater. **48**, 647–652 (2003)
20. H.A. Patel, D.L. Chen, S.D. Bhole, K. Sadayappan, J. Alloy. Compd. **496**, 140–148 (2010)
21. I.A. Yakubtsov, B.J. Diak, C.A. Sager, B. Bhattacharya, W.D. MacDonald, M. Niewczas, Mater. Sci. Eng. A **496**, 247–255 (2008)
22. A. Zindal, J. Jain, R. Prasad, S.S. Singh, P. Cizek, Mater. Sci. Eng. A **706**, 192–200 (2017)
23. S. Chang, J.E. Morral, Acta Metall. **23**, 685–689 (1975)
24. ASTM E8/E8M-04, *Standard Test Methods for Tension Testing of Metallic Materials* (American Society for Testing and Materials, West Conshohocken, PA, United States, 2015)
25. D.A. Porter, K.E. Easterling, *Phase Transformations in Metals and Alloys* (Chapman & Hall, London, 1992)
26. L.R. Gill, G.W. Lorimer, P. Lyon, Adv. Eng. Mater. **9**, 784–792 (2007)
27. D. Duly, J.P. Simon, Y. Brechet, Acta Metall. Mater. **43**, 101–106 (1995)
28. A. Zindal, J. Jain, R. Prasad, S.S. Singh, R. Sarvesha, P. Cizek, M. Barnett, Mater. Charact. **136**, 175–182 (2018)
29. J.B. Clark, Acta Metall. **16**, 141–152 (1968)
30. C.H. Caceres, C.J. Davidson, J.R. Griffiths, C.L. Newton, Mater. Sci. Eng. A **325**, 344–355 (2002)
31. T. Kawabata, O. Izumi, J. Mater. Sci. **11**, 892–902 (1976)